Effects of radiative cooling on the tropical convective response to sea surface temperature: 2-D large domain cumulus ensemble simulations

C.-H. Sui,[1] X. Li,[2] C.-H. Ho,[3] and K.-M. Lau[4]

Received 16 February 2007; revised 25 October 2007; accepted 13 December 2007; published 25 April 2008.

[1] The effects of radiative cooling on the tropical convective response to sea surface temperature (SST) are investigated using a series of two-dimensional large domain cloud-resolving simulations. The experiments are designed with an imposed warm-pool SST at 2.5°C, 3.5°C, and 4.5°C higher than the cold-pool SST, which is specified at 26°C. The area ratio of the model cold pool to the warm pool is set to 2.2. It is observed that the warm-pool convection intensifies when the SST difference between the warm and cold pools increases from 2.5°C to 3.5°C, whereas the warm-pool convection strength does not significantly change when the SST difference increases from 3.5°C to 4.5°C, which is qualitatively consistent with the observations. The analysis of the atmospheric heat budgets shows that the cap on the development of convection over the warm pool is due to a radiative cooling over the cold pool that has a small variability. The cloud-resolving model simulations indicate that the area of the radiatively driven subsidence expands to produce an enhanced mass exchange between the warm and cold pools in response to the enhanced SST difference between them. This acts against the tendency for increased clouds by the enhanced upward mass flux in response to the warmer SST over the warm pool; significantly stronger SST differences between the two pools (e.g., ≥3.5°C in the cloud-resolving model) do not proportionally produce further intensive convection activities over the warm pool.

Citation: Sui, C.-H., X. Li, C.-H. Ho, and K.-M. Lau (2008), Effects of radiative cooling on the tropical convective response to sea surface temperature: 2-D large domain cumulus ensemble simulations, *J. Geophys. Res.*, *113*, D08116, doi:10.1029/2007JD008557.

1. Introduction

[2] The tropical Pacific Ocean - atmosphere is a primary component of the Earth climate system that consists of warm pool (>28°C) in the western Pacific, cold pool (<24°C) in the eastern Pacific, easterly trade winds near the surface, and a reversed flow in the upper troposphere. The warm pool and cold pool fluctuates at interannual timescale known as El Nino phenomenon, otherwise the east-west contrast of sea surface temperature (SST) is quite stable climatologically. This climate system is maintained by coupled ocean-atmosphere dynamics so the change of trade winds affects the east-west SST gradient which in turn affects atmospheric circulation and water vapor/clouds. The change of water vapor and clouds further affects climate through radiative forcing.

[3] Many observational analyses and general circulation model (GCM) simulations show that the area-mean greenhouse trapping of the clear-sky in the tropics generally increases from cold to warm SST [e.g., *Zhang et al.*, 1996; *Soden*, 1997; *Inamdar and Ramanathan*, 1994]. These studies generally support a positive water vapor feedback on overall climate warming. However, *Chou* [1994] found the area-mean clear-sky greenhouse effect was smaller during the warmer month of April 1987 than during the colder month of April 1985. The observed decrease in greenhouse trapping with increased surface temperature was most evident over the dry subtropical regions. Chou's analysis reveals that the change in the relative area of dry and subsiding versus moist and convective regions determines the sign of area-mean clear sky water vapor greenhouse trapping. This is in line with the argument by *Lindzen* [1990] about a possible negative water vapor feedback to the global warming. By considering the tropical heat budget, *Pierrehumbert* [1995] emphasized that the tropical climate is mainly determined by the clear-sky water vapor greenhouse effect averaged over the entire tropics. He considered the water vapor and convection over the tropical warm pool as a furnace, and the radiative cooling in the subsidence region as a fin. The radiator fin regulates the tropical SST and prevents the tropical climate from entering a runaway greenhouse state.

[4] Being inseparable from water vapor feedback, cloud-radiative forcing is another important climate feedback process. However, the effect of cloud feedback on climate change is controversial. Studies of cirrus (or high) clouds

[1]Institute of Hydrological and Oceanic Sciences and Department of Atmospheric Sciences, National Central University, Jhongli, Taiwan.
[2]NOAA/NESDIS/Center for Satellite Applications and Research, Camps Springs, Maryland, USA.
[3]School of Earth and Environmental Sciences, Seoul National University, Seoul, Korea.
[4]NASA/GSFC/Laboratory for Atmospheres, Greenbelt, Maryland, USA.

Copyright 2008 by the American Geophysical Union.
0148-0227/08/2007JD008557

and associated radiative effect on tropical climate do not even agree on the sign of the cloud feedbacks [e.g., *Prabhakara et al.*, 1993; *Ramanathan and Collins*, 1991; *Kiehl*, 1994]. *Lindzen et al.* [2000] showed observational evidence that area-mean clouds over the warm pool reduces by about 15% for a 1°C increase of the cloud-weighted sea surface temperature (SST). The radiative implications of the observed cloud-SST relation are assessed in a simple radiative-convective model that shows a negative feedback in the global climate.

[5] A synthesis of the above studies reveals that water vapor and clouds feedbacks depend on the relative areas of cloudy/moist regions versus clear/dry regions, as well as on cloud properties (type, height, optical thickness) and water vapor distribution within the clear and cloudy regimes. Analyzing or modeling these feedback processes are still challenging research because of limited observations and highly parameterized hydrologic processes in most climate models.

[6] To gain a better knowledge of the role of water vapor/cloud - radiative interaction in tropical climate, cloud-resolving models have been used to study tropical equilibrium states subject to different SSTs because of the explicit treatment of convective-radiative processes [e.g., *Held et al.*, 1993; *Sui et al.*, 1994; *Grabowski et al.*, 1996; *Tao et al.*, 1999; *Xu and Randall*, 1999]. *Lau et al.* [1993] applied the same cloud-resolving model as that used by *Sui et al.* [1994] to study the convective-radiative equilibrium of the model to several perturbed climate conditions in the tropics. *Sui et al.* [1993] and *Lau et al.* [1994] applied the cloud-resolving model results to explain the observational analysis by *Ramanathan and Collins* [1991]. They found that the change in cloud radiative forcing induced by the local surface warming in the model is one order of magnitude smaller than that induced by the changes in the large-scale circulation. Therefore they argued that both local processes and large-scale dynamics should be considered in the study of cloud feedbacks. *Tompkins and Craig* [1998] used a three-dimensional (3-D) cloud-resolving model to study the sensitivity of tropical convection-radiation to SST in the absence of large-scale flows. Their major conclusion is consistent with those of *Sui et al.* [1993] and *Lau et al.* [1994]; however, they have emphasized on the microphysics aspects of the results.

[7] An obvious limitation of the cloud-resolving modeling studies by *Sui et al.* [1993] and *Lau et al.* [1993, 1994] in the study of cloud/water vapor responses to SST changes is the absence of large-scale feedback between the tropical convective regime (warm pool) and the surrounding subsidence regime (cold pool). One important aspect of the large-scale feedbacks between the two regimes is the contribution of radiative cooling in the broad subsidence regime to the net water vapor feedback effect, as discussed above.

[8] In this study, the SST difference is permitted in the two dimensional (2-D) cloud ensemble model (CEM) so that an SST gradient-induced walker-type circulation is generated to interact with clouds through convective-radiative processes. This study aims to resolve how the warm and cold pools communicate with each other and which physical process caps the vertical motion as the SST difference increases. Therefore a series of sensitivity tests are carried out using a CEM and the heat and moisture budgets are analyzed over the warm and cold pools. The model and experimental designs of this study are discussed in section 2. The equilibrium solution of a control experiment is described in section 3. The tropical convective response to SST is examined by perturbing the SST in the warm pool, and the effect of radiative cooling in the cold pool on the response is analyzed in section 4. Some supporting evidence for the model results are discussed in section 5 based on observations. The results are summarized in section 6.

2. Model and Experiments

[9] The CEM used in this study was developed at Goddard Space Flight Center. The model was originally based on a model developed by previous researches [e.g., *Soong and Ogura*, 1980; *Soong and Tao*, 1980; *Tao and Soong*, 1986; *Tao and Simpson*, 1993]. The model consists of a nonhydrostatic and anelastic set of equations for the potential temperature (θ), water vapor mixing ratio (q_v), and winds (u, v, and w). The model's cloud microphysics includes a parameterized Kessler-type two-category (cloud water and rain) liquid water scheme and parameterized three-category (i.e., cloud ice, snow, and hail/graupel) ice-phase schemes. The saturation adjustment scheme for removing supersaturated vapor or sub-saturation in the presence of clouds was described by *Tao et al.* [1989]. For the treatment of subgrid-scale turbulence, a prognostic equation is solved for the subgrid kinetic energy that is then used to specify the eddy coefficients. The heat and moisture fluxes at the sea surface are obtained from the bulk formulation. A detailed description and references about the bulk formulation can be found by *Tao and Simpson* [1993]. The 2-D version of the model used by *Sui et al.* [1994, 1998] with modified treatments of radiative processes and cloud microphysics [*Li et al.*, 1999, 2002] is used here. The modified model has been demonstrated by *Li et al.* [1999] to produce better simulations in response to the imposed large-scale forcing as evaluated against the Tropical Ocean Global Atmosphere-Coupled Ocean Atmosphere Response Experiment (TOGA-COARE) observations. A more updated description of the model microphysics, radiation, and surface processes in the CEM is provided by *Tao et al.* [2003].

[10] The model has 31 vertically stretched levels with the highest level at 21 km. Rayleigh damping with a coefficient that increases with height is used above 16 km to reduce the upper boundary reflection. Experiments are performed in an ocean domain of 5120 km (Δx = 2.5 km) along the equator with an idealized top-hat SST distribution of a warm pool that is approximately 1588 km wide in the center and a cold pool on both sides. The corresponding area ratio of the cold pool to the warm pool is 2.2. In nature, the ratio varies in different warm scenarios due to atmosphere and ocean interaction. In atmospheric models, we must prescribe SST as lower boundary condition. There are different ways to prescribe SST gradient in a model. In this study, we choose to fix the area ratio but change the warm pool-cold pool SST contrast.

[11] The available computation power limits us to choose relatively coarse horizontal and vertical resolutions as a compromise to the large domain size in the current experiments. However, the model with such resolution can still

Table 1. Imposed SSTs (°C) in All Experiments

	Warm Pool	Cold Pool
R2	30.5	26
R1	29.5	26
R	28.5	26

produce reasonable cloud properties as demonstrated in a study of the response of deep tropical clouds to large-scale thermodynamic forcings by *Johnson et al.* [2002]. They performed a systematic comparison of forced 2D experiments using essentially the same Goddard CEM of different horizontal and vertical resolutions. Some other sensitivity test by Dr. Wei-Kuo Tao at Goddard Space Flight Center indicates that the model is less sensitive to resolution if the large-scale forcing is imposed.

[12] Three experiments are performed with the warm-pool SST specified at 28.5°C, 29.5°C, and 30.5°C respectively, and the cold-pool SST at 26°C. These three experiments are designed to study the effect of radiation-dynamic interaction on tropical climate in the presence of large-scale circulation adjustments (section 4) and are denoted as R, R1, and R2, as listed in Table 1.

[13] An important model design in this study is to introduce a heat sink and moisture source, in order to produce thermodynamic and cloud properties similar to the observed tropical atmosphere. We achieved this purpose by imposing a time- and horizontal-independent vertical profile of upward motion in the model that gives rise to a moisture source and a heat sink [*Li et al.*, 1999]. The same profile of the mean upward motion is imposed in all experiments (see discussions later).

[14] One may wonder the sensitivity of the results to the setups of experiments, like the specified area ratio and the imposed vertical distributions of upward motion. We there fore carried out two more experiments with zero vertical velocity and an imposed vertical motion that is twice the magnitude of the R, R1, and R2. The results (summarized in section 5 below) show that the major conclusion of the present study is not sensitive to the experimental setups.

[15] Integration begins from an atmosphere at rest with zonally uniform temperature and the moisture obtained from the observed mean values over the western Pacific. Clouds are initially absent. All experiments are integrated for 50–70 days to attain an equilibrium state.

3. Equilibrium Solution of Control Experiment

[16] Figure 1 shows the temporal evolution of mass-weighted column-mean temperature and precipitable water (column-total specific humidity) over the warm and cool pools, respectively, for the control experiment (R1). The model attains the equilibrium state in approximately 15 days. The equilibrium solution is characterized by a moist state over the warm pool, a dry state over the cold pool, and almost the same column-mean temperature in the two regimes. The equilibrium state is a result of the walker-type circulation induced by the SST contrast such that air ascends over the warm pool and descends over the cold pool, as revealed by the time- and area-mean vertical motion over the two regimes derived from model-calculated vertical velocity at each model grid point from R1 for the period from day 40 to day 50 (Figure 2). The mean upward motion over the warm pool is approximately one order of magnitude larger than the mean downward motion over the cold pool. Figure 2 also shows a weak upward motion near 200 hPa over the cold pool maintained by the cloud-radiative heating due to the existence of ice clouds (see the discussions below about Figures 3b and 4a). The vertical motion over the warm pool is maintained by the latent heat released by deep convection, as revealed by the mean rainfall over the warm pool shown in Figure 1. On the other hand, rainfall is nearly absent over the cold pool due to the prevailing downward motion. It is also found that the temperature distribution shows that the largest difference in the lapse rates between the two pools exists in the lower troposphere (not shown), where the cold pool is stable while the warm pool is unstable. This indicates that the stability effectively prevents the development of convection in the cold pool.

[17] The model heat and moisture budgets are shown in Figure 3 from R1. The heat budget in the warm pool (Figure 3a) shows the well-known fact that condensation heating and advective cooling are dominant in the heat budget. However, since these processes almost balance each other, their residue almost balances the radiation. The radiative heating (cooling) in the middle (upper) troposphere may reflect the effect of high clouds. In contrast to the warm-pool budget, the heat budget in the cold pool (Figure 3b) is balanced between radiative cooling and advective warming

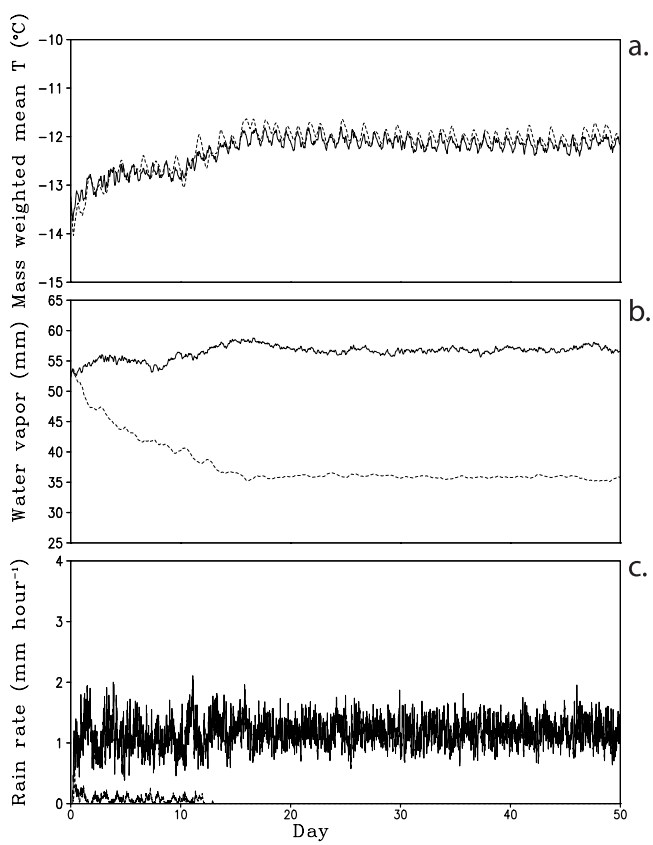

Figure 1. Time series of vertically averaged temperature (a) and moisture (b) and surface rainfall rate (c) over the warm pool (solid curves) and cold pool (dashed curves) from R1.

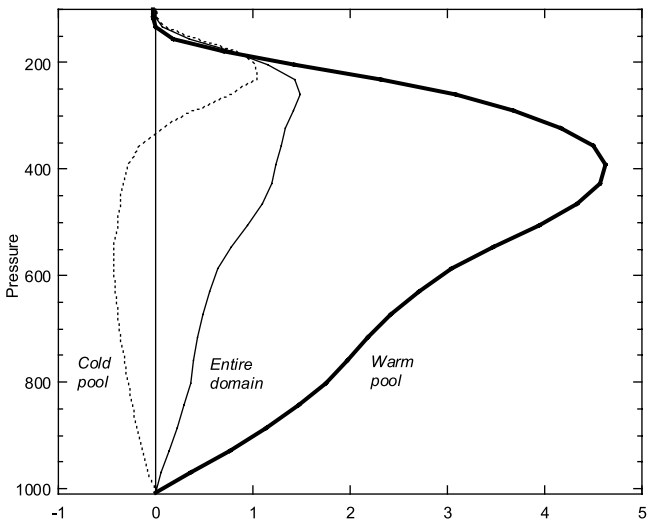

Figure 2. The profile of vertical velocity over the entire domain (thin solid) is specified in all experiments, and the time- and area-mean profiles of vertical velocity over the warm pool (thick solid) and cold pool (dashed) are derived from model-calculated vertical velocity at each model grid point during the period from day 40 to 50, from R1. Unit is cm s^{-1}.

in the entire troposphere except near 200 hPa where the two terms have an opposite sign due to the presence of ice clouds (see Figure 4a). The presence of the ice clouds also contributes to evaporative cooling near 500 hPa. The heat budget indicates that while the condensational heating and thermal advection are the two dominant processes in the warm pool, the radiative process is crucial for maintaining the heat balance in the cold pool. Therefore the radiative cooling in the cold pool plays an important role in maintaining the equilibrium since it determines the subsidence in the cold pool, which in turn affects the ascending motion in the warm pool.

[18] Sources of water vapor over the cold pool include evaporation from the sea surface and the clouds advected from the surrounding regions. The moisture budget in the cold pool for R1 is shown in Figure 3c. The figure shows a moistening peak by advection near 250–400 hPa, a moistening peak by evaporation near 550 hPa, and a drying peak by condensation near 200 hPa. These peaks are balanced by the vertical eddy flux convergence. The most likely explanation for these sources and sinks is that water vapor is advected from the warm pool to the cold pool in the upper troposphere (above 450 hPa) where it forms ice clouds that are maintained by the unstable temperature stratification due to the cloud-radiative effect. Most falling ice clouds (snow and graupel) quickly change into vapor through sublimation and evaporation in a thin layer near 550 hPa because the lower troposphere below 450 hPa is dry. Some of the ice clouds melt and fall to lower troposphere as light rain.

[19] The above explanation is supported by the fields of cloud, water vapor anomalies, zonal wind, and vertical

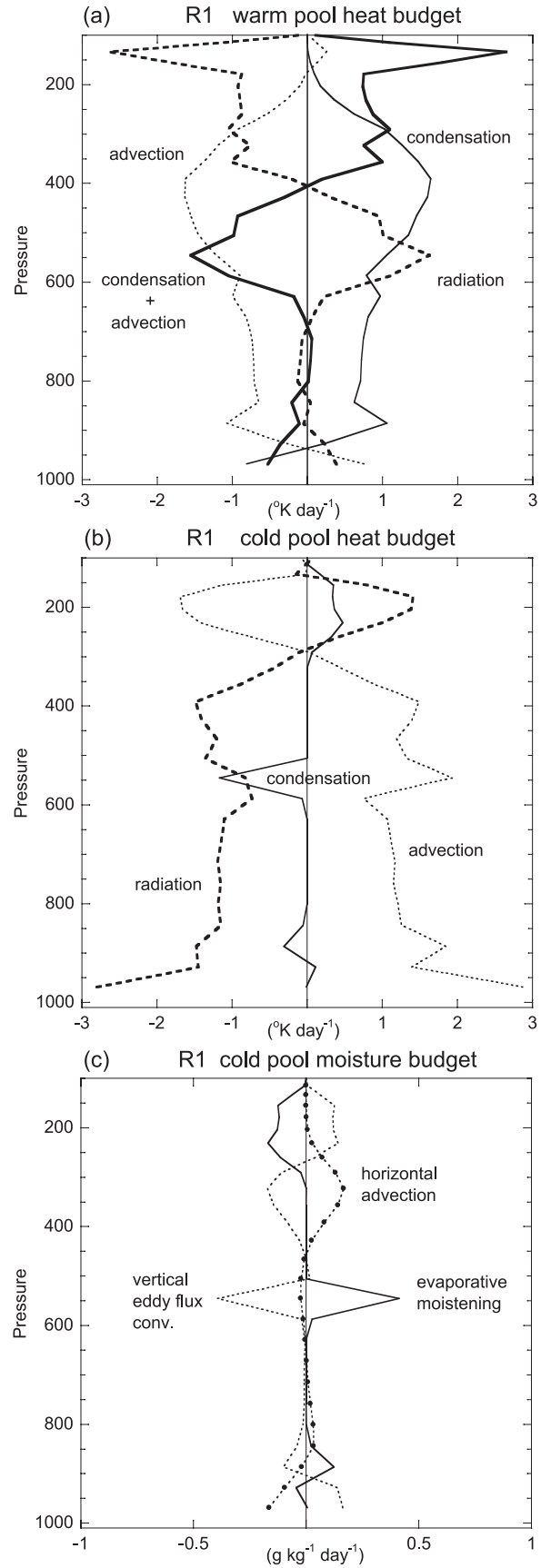

Figure 3. Time-mean heat budgets averaged over the warm pool (a) and the cold pool (b) and the time mean moisture budget over the cold pool (c) from R1. Note that the scales of condensation heating and vertical advection are 10 times larger than those of the other two terms in Figure 3a.

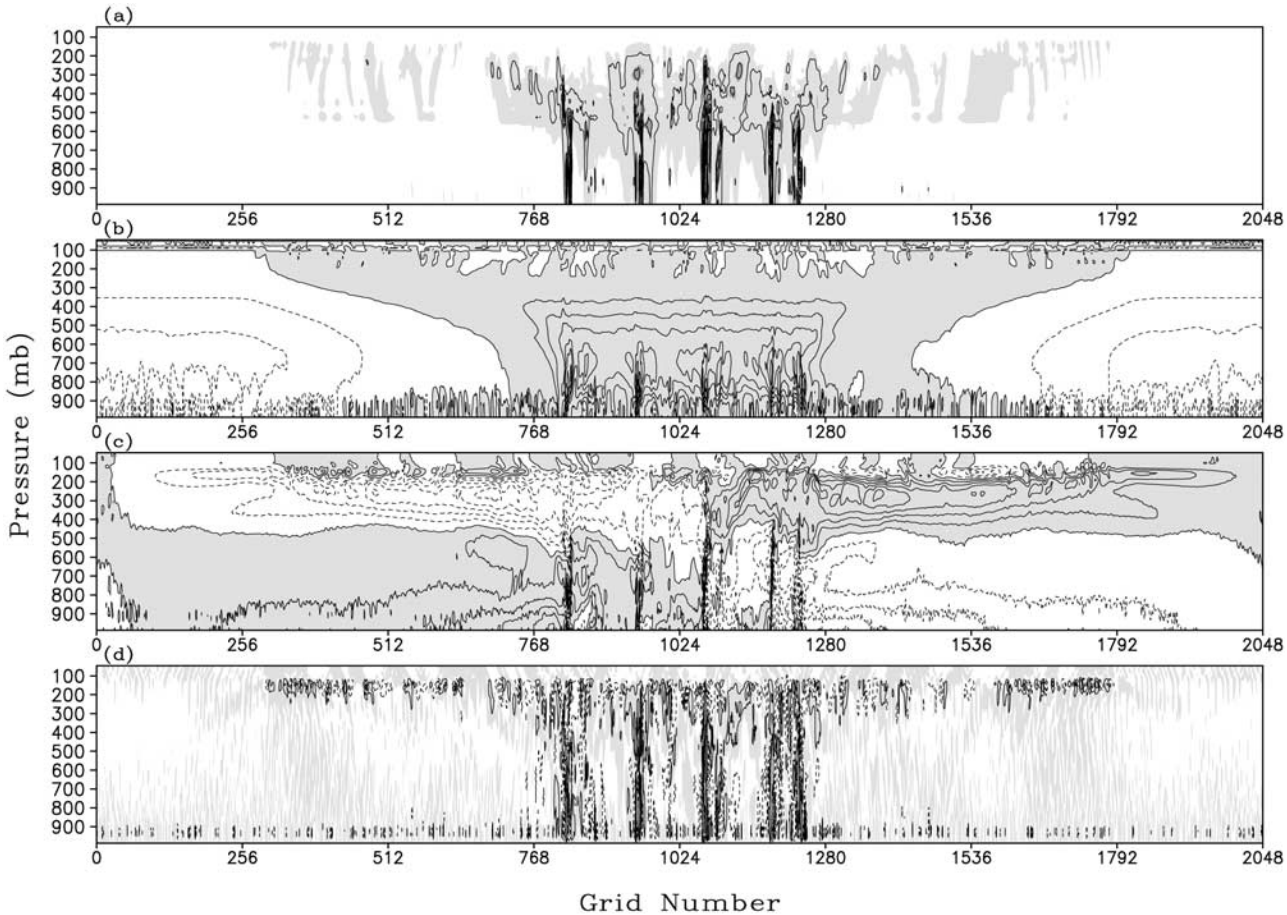

Figure 4. Snap shot of (a) total cloud content, q_c, (b) perturbation water vapor mixing ratio, q_v', (c) zonal wind, u, and (d) vertical velocity, w at Day 40 from R1. In the above figures, areas of $q_c > 10^{-3}$ g kg^{-1} and positive q_v', u, and w are shaded. Contour intervals of q_c, q_v', u, and w are, respectively, 0.04 g kg^{-1} starting at 0.01 g kg^{-1}, 2 g kg^{-1}, 2 m s^{-1}, and 20 cm s^{-1} starting at ±10 cm s^{-1}, respectively.

motion at day 40, as shown in Figure 4. These figures show major convective cores over the warm pool in the central domain which are associated with deep clouds (Figure 4a), strong updrafts/downdrafts (Figure 4d), and the extensive upper-level moisture anomalies (Figure 4b) due to the upper-level divergent and low-level convergent circulation (Figure 4c). These major convective cores contribute to the warm-pool mean upward motion (Figure 2). The upper-level moisture is the source of the ice clouds extending outward from the warm pool to the cold pool where they disappeared at around 550 hPa (Figure 4a). This is the same level where evaporation appears in the water vapor budget (Figure 3c). The spatial structure of the upper-level ice clouds, water vapor, and zonal winds above 300 hPa over the cold pool shows the existence of convective updrafts and downdrafts, indicating a strong radiative-convective interaction. This is consistent with the radiative heating distribution in the upper troposphere shown in Figure 3b. Boundary layer clouds ($q_c < 10^{-3}$ g kg^{-1}) associated with relatively weaker updrafts/downdrafts ($|w| < 20$ cm s^{-1}) also appear below 900 hPa in the entire domain (Figures 4a and 4d). The shallow and deep convection initiate many gravity waves as shown by the vertical motion in Figure 4d.

[20] One may question the realism of the vertical motion in the upper troposphere over the cold pool in the model results because of parameterized cloud physics and idealized experiment designs (e.g., 2D-configuration, prescribed large scale updraft) of this model study. This remains an issue for future study as the direct measurements become available.

4. Perturbed Equilibrium Solutions

[21] We now examine the response of an equilibrium solution to the increasing SST contrasts in experiments R, R1, and R2 with the warm pool SST at 2.5°C, 3.5°C, and 4.5°C, respectively, warmer than the cold pool SST. Table 2 shows that with the increase in SST from R to R1, the mean surface rainrate over the entire domain (the total rainrate) increases from 0.36 mm h^{-1} to 0.37 mm h^{-1} (i.e., +1.6%),

Table 2. Precipitable Water in Warm (PW_W) and Cold (PW_C) Pools, Mean Rain Rate (RR), Rainy Area (RA), and Rain Intensity (RI) Over the Entire Domain Simulated in Experiments R, R1, and R2

Experiment	PW_w, mm	PW_C, mm	RR, mm h^{-1}	RA, %	RI, mm h^{-1}
R2	53.60	31.58	0.39	22	1.73
R1	52.47	32.35	0.37	25	1.45
R	48.36	33.95	0.36	44	0.82

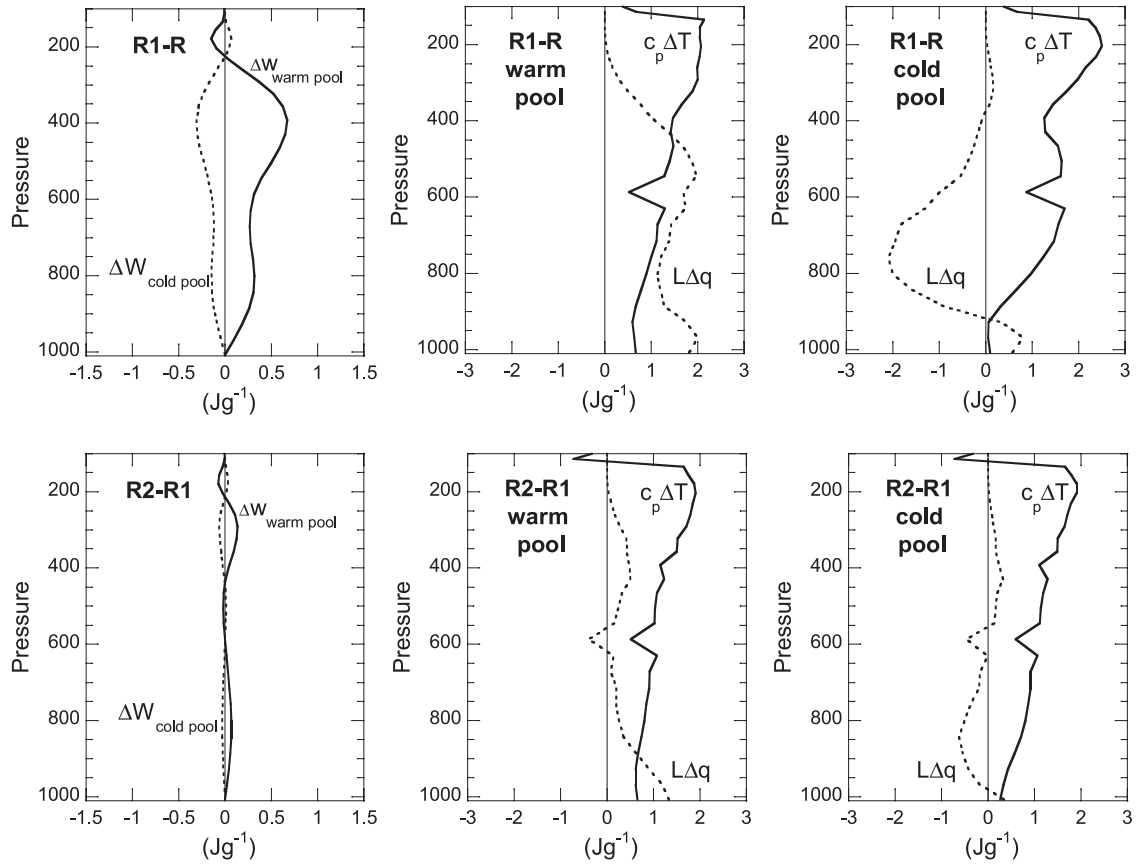

Figure 5. Vertical profiles of the difference in c_pT, Lq_v, and w for R1 minus R (upper) and R2 minus R1 (lower) averaged over the warm and cold pools. Units of c_pT and Lq_v are J g^{-1} and w is in cm s^{-1}.

while the mean rainy area decreases from 44% to 25% (i.e., −43%). Therefore the mean surface rainrate over the rainy area (rainrate intensity) increases from 0.82 mm h^{-1} to 1.45 mm h^{-1} (i.e., +79%). The enhanced rainrate intensity indicates a stronger mean upward motion as expected by the enhanced SST contrast. However, the total rainrate, rainy area, and rainrate intensity for R2 are 0.39 mm h^{-1}, 22%, and 1.73 mm h^{-1}, respectively; therefore, the fractional change in the rainrate intensity from R1 to R2 is only 20%, which is significantly weaker than the value from R to R1. This indicates a nonlinear response to the increasing SST contrast due to the regulating role of radiative cooling, which is discussed below.

[22] We then examine the difference in the ensemble mean temperature, specific humidity, and vertical velocity in the two regimes for R1 and R (Figure 5, upper panels). The results indicate that the mean upward (downward) motion increases in the warm (cold) pool as the SST contrast increases from 2.5°C to 3.5°C. This leads to a more humid atmosphere in the warm pool and a drier atmosphere (except in the boundary layer and the upper troposphere near 300 hPa) in the cold pool. The much drier atmosphere in the cold pool in R1 relative to R is due to the difference in convective area in terms of raining area (Table 2). The mean raining area for the integration period of 40–50 day in R (44% of the domain) is larger than the warm pool (31% of the domain). Thus the area-mean moisture over the cold pool includes portion of the convective atmosphere. On the other hand, the mean raining area in R1 (25% of the domain, respectively) is confined within the warm pool, and the area-mean moisture over the cold pool is much drier relative to R. Figure 5 (upper panels) further shows that the equilibrium air temperature in both regimes increases, indicating the effect of overall warming by subsidence in response to the enhanced convective updraft.

[23] As the SST contrast increases from 3.5°C to 4.5°C from R1 and R2, the mean temperature and humidity differences between R2 and R1 (Figure 5, lower panels) are slightly weaker than those between R1 and R; however, the mean vertical motion remains almost unchanged from R1 to R2. This is remarkable since the averaged rain intensity over the warm pool increases by 20% from R1 to R2, as discussed above. However, Table 2 shows that the precipitation falls over a narrower area in R2 than in R1, which is the main cause for the increase in the rain intensity from R1 to R2. Therefore the nearly identical vertical motion between R2 and R1 reflects the fact that the convective regions over the warm pool become smaller and stronger with the increasing SST contrast, and the cloud-free areas within the warm pool become larger. The cause of the decrease in the convective areas with increasing SST contrast can be explained by the heat budgets in the cold pool region, as discussed below.

[24] The differences in the heat budget in the cold pool for R1 minus R and R2 minus R1 are shown in Figure 6. The figure shows that the differences in the radiative cool-

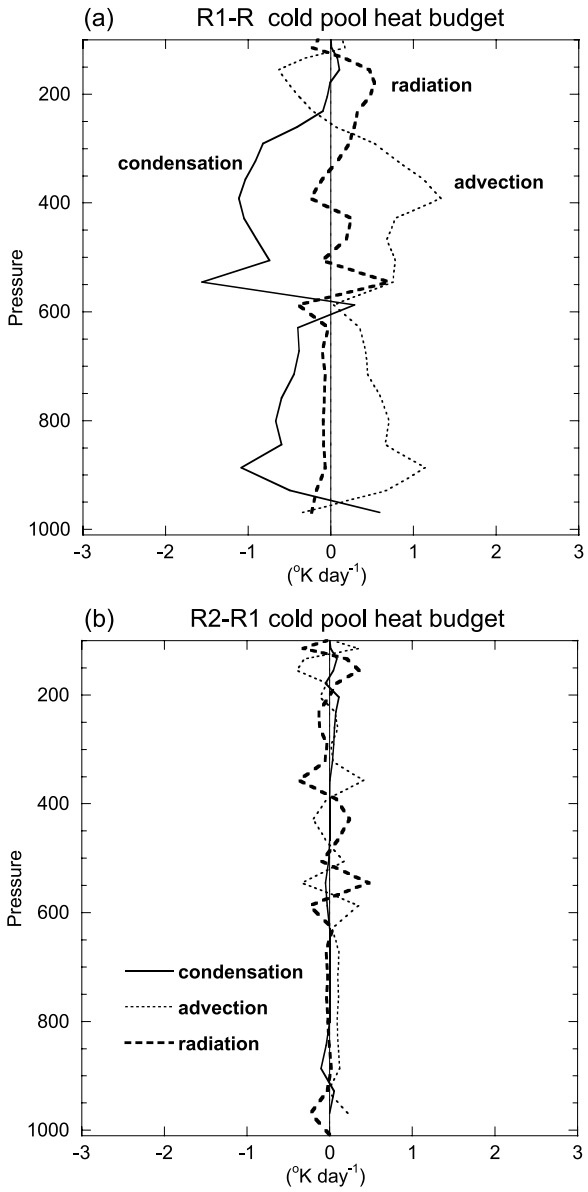

Figure 6. Vertical profiles of the difference in the heat budget for R1 minus R (a) and R2 minus R1 (b).

ing in the cold pool between R and R1 and between R2 and R1 are quite small, indicating that it remains virtually unchanged in all three experiments. As discussed above, the existence of latent heating in the cold pool only occurs in R since the SST contrast is weak (2.5°C), and not in R1 and R2. Therefore the difference between the area-mean heat budget over the cold pool in R1 and R is balanced between a reduced condensation heating and reduced adiabatic cooling; however, the area-mean subsidence warming does not change significantly in R, R1, and R2 in the absence of latent heating. This indicates that the radiative cooling effectively caps the magnitude of the subsidence motion, consistent with a common knowledge that the flow field is controlled by radiative cooling [e.g., *Iwasa et al.*, 2002]. Consequently, to produce an enhanced mass exchange between the warm pool and the surrounding cold pool in response to the enhanced SST contrast, the amplitude of subsidence remains unchanged but the area of subsidence expands to produce more downward mass flux to balance more upward mass flux.

5. Discussion

[25] In this section, we seek supporting evidence for the model result. First, we assess whether the simulated thermodynamic states in R, R1, and R2 are similar to the observed tropical atmosphere. Since these experiments are sensitive to the imposed domain-mean vertical velocity, we also performed two experiments similar to R1 but one with twice the amplitude of the imposed vertical velocity (CW) and the other with zero vertical velocity (CNW). The vertical and areal mean temperature, T, and specific humidity, q_v, (expressed in units of J kg^{-1} by multiplying specific heat c_p and latent heat constant L, respectively) of these experiments in the warm pool and cold pool are shown in Figure 7a. We also estimate the vertical and areal mean thermodynamic states in the warm pool and cold pool using an updated reanalysis data produced by the National Centers for Environmental Prediction (NCEP)/National Center for Atmospheric Research (NCAR) [*Kalnay et al.*, 1996; *Kanamitsu et al.*, 2002] and the European Centre for

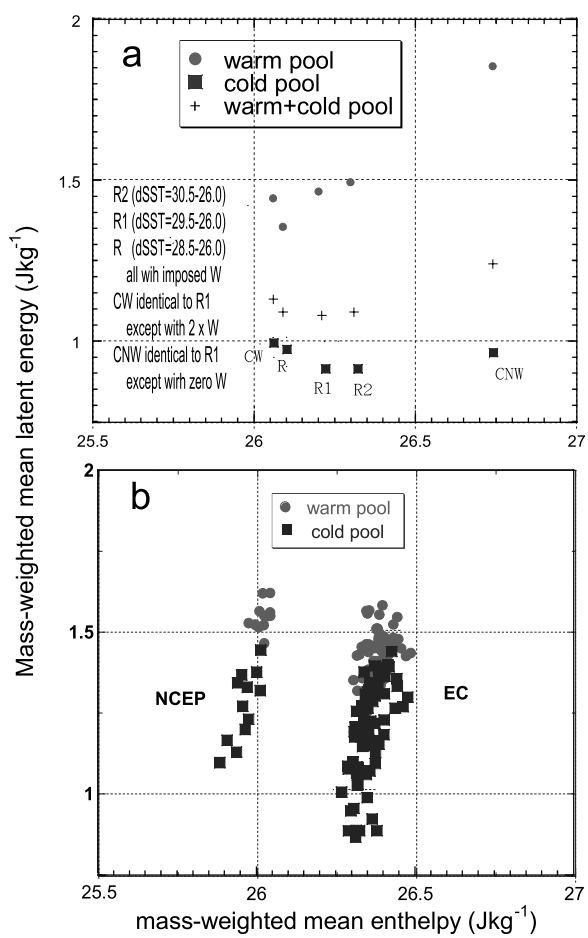

Figure 7. Area and vertical mean c_pT and Lq_v over the warm pool and cold pool from the model experiments R, R1, R2, CW and CNW (a), and from the monthly mean values in 1995 from the NCEP and ERA reanalysis (b). Unit is (J kg^{-1}).

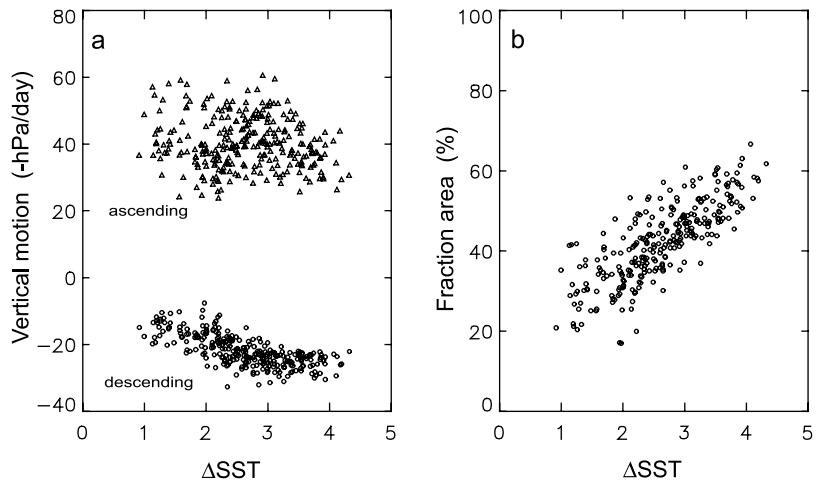

Figure 8. The monthly mean values of (a) $-\omega_{500}$ (hPa day^{-1}) averaged over the descending region and ascending region versus the difference between SST in the warm and cold pools within 130°E–110°W and 10°S–10°N (ΔSST); (b) fractional area of descending motion (%) at 500 hPa versus ΔSST. Data is derived from NCEP-NCAR reanalysis for the period of 1982–2004.

Medium-Range Weather Forecasts (ECMWF) [*Gibson et al.*, 1996, 1997] on a 2.5° × 2.5° grid resolution. The tropical Pacific within (130°E–110°W, 10°S–10°N) is selected for the calculation. Within the domain, the warm and cold pools are separated by an isotherm determined in such a manner that the area of the warm pool is 25% of the total area. The vertical and areal mean c_pT and Lq_v in the warm pool and cold pool derived from both reanalysis data for the year 1995 are shown in Figure 7b. The model results derived from R, R1, R2, and CW with imposed domain-mean vertical velocity are all within observed range of observed thermodynamic states. However, the results from CNW (imposed zero domain-mean vertical velocity) are quite different from observations.

[26] Next, we analyze the monthly mean data from the NCEP-NCAR reanalysis and the monthly mean SST data from NCEP [*Reynolds and Smith*, 1994] to estimate the vertical velocity in the pressure coordinate at 500 hPa (ω_{500}) averaged over the descending region and ascending region as a function of the SST difference between the warm pool and cold pool (ΔSST). The warm and cold pools are similarly defined in the tropical Pacific within (130°E–110°W, 10°S–10°N) as discussed above. The monthly mean values of $-\omega_{500}$ averaged over the descending region and ascending region for the period of 1982–2004 are plotted in Figure 8 against ΔSST. We also show in Figure 8 the fractional area of descending motion within the tropical Pacific region (130°E–110°W, 10°S–10°N) as a function of ΔSST.

[27] The figure shows that the fractional area of descending motion generally increases with increasing ΔSST, and the mean descending motion also shows an increasing trend with dSST but only for ΔSST < 3°C. For ΔSST > 3°C, the mean descending motion remains unchanged with increasing ΔSST. This appears to be consistent with the different model response to weaker lower boundary forcing (R to R1) and stronger lower boundary forcing (R1 to R2). However, the mean ascending motion does not show a clear relation with ΔSST in Figure 8. The lack of correlation can be explained by the fact that, unlike the model experiments, the mean vertical motion in the domain of analysis varies month by month and is expected to influence the vertical motion-ΔSST relation. We can multiply the monthly mean ascending and descending motion by a factor to adjust the domain mean vertical motion to a common value. The adjusted ascending motion is indeed positively correlated with ΔSST (figure not shown), supporting our model results.

[28] Although the above results of reanalysis data appear to support our model results, we recognize that the tropical Pacific is not an isolated climate system like the model world. The 2D experiments are also just an idealization of the 3D tropical Pacific climate system where the basin-scale SST distribution and the area mean vertical motion are affected by interannual and lower-frequency oscillations. Therefore the model response should be understood with these limitations in mind.

6. Summary

[29] The regulation of radiative cooling in the SST gradient-induced tropical convection is examined using a 2-D cloud-resolving model. The experiments are conducted by integrating the model over an ocean domain of 5120 km with an imposed mean vertical motion and idealized SST distributions of a warm pool that is approximately 1588 km wide at the center and a cold pool in the rest of the domain. For each experiment, the model is integrated for 50–70 days to attain the equilibrium state. A mean ascending motion over the warm pool and a descending motion over the cold pool are developed in each of the simulations.

[30] In experiments R, R1, and R2, the warm pool SST is at 2.5°C, 3.5°C, and 4.5°C, respectively, warmer than the cold pool SST, which is at 26°C. The most notable difference among the three experiments is the mean upward motion over the warm pool and the mean downward motion over the cold pool that increases appreciably as the SST contrast changes from 2.5°C to 3.5°C, but remains almost unchanged as the SST contrast changes from 3.5°C to 4.5°C. This can be explained by the heat budget in the subsidence regime that is balanced between the radiative

cooling and subsidence warming. Since the radiative cooling in the subsidence regime remains almost constant in all three experiments, it caps the subsidence warming. In response to the increasing SST contrast, the subsidence expands its area instead of increasing its magnitude. The area-mean subsidence warming over the cold pool from R to R1 appears enhanced because of the increased subsidence area. From R1 to R2, the subsidence area further expands into the warm pool region when the warm pool SST exceeds 29.5°C, and the area-mean subsidence warming over the cold pool no longer changes due to the absence of condensation heating. Therefore the mean downward motion over the cold pool remains unchanged.

[31] The present study demonstrates a possible regulation effect of radiative cooling on tropical circulation. The idealized experiments also provide a way to quantify the water vapor and cloud feedbacks under controlled conditions. Yet we must be cautious to apply the results for understanding changes of water vapor- and cloud-radiative forcing in nature or climate models because of the limitations of the idealized model experiments as discussed in the previous section.

[32] **Acknowledgments.** The authors thank W.-K. Tao at NASA/GSFC for his cloud-resolving model and Myung-Sook Park for analyzing ERA and NCEP reanalysis data to make Figure 8. C.-H. Sui was supported by the National Sciences Council in Taiwan under grants NSC 095-2111-M-008-003 and NSC 094-2111-M-008-008. C.-H. Ho was supported by the CATER 2006-4204.

References

Chou, M. D. (1994), Coolness in the tropical Pacific during an El Nino episode, *J. Clim.*, *7*, 1684–1692.

Gibson, J. K., P. Kallberg, and S. Uppala (1996), The ECMWF ReAnalysis (ERA) project, *ECMWF Newslett.*, *73*, 7–17.

Gibson, J. K., P. Kallberg, S. Uppala, A. Hernandez, A. Nomura, and E. Serrano (1997), ECMWF ReAnalysis Project Rep. Ser. 1, ECMWF, Shinfield Park, Reading, United Kingdom, 72 pp.

Grabowski, W. W., M. W. Moncrieff, and J. T. Kiehl (1996), Long-term behaviour of precipitating tropical cloud systems: A numerical study, *Q. J. R. Meteorol. Soc.*, *122*, 1019–1042.

Held, I. M., R. S. Hemler, and V. Ramaswamy (1993), Radiative-convective equilibrium with explicit two-dimensional moist convection, *J. Atmos. Sci.*, *23*, 3909–3927.

Inamdar, A. K., and V. Ramanathan (1994), Physics of greenhouse effect and convection in warm oceans, *J. Clim.*, *7*, 715–731.

Iwasa, Y., Y. Abe, and H. Tanaka (2002), Structure of the atmosphere in radiative-convective equilibrium, *J. Atmos. Sci.*, *59*, 2197–2226.

Johnson, D., W.-K. Tao, J. Simpson, and C.-H. Sui (2002), A study of the response of deep tropical clouds to mesoscale processes: Part I: Modeling strategies and simulations of TOGA-COARE convective systems, *J. Atmos. Sci.*, *59*, 3492–3518.

Kalnay, E., et al. (1996), The NMC/NCAR 40 year reanalysis project, *Bull. Am. Meteorol. Soc.*, *77*, 437–471.

Kanamitsu, M., W. Ebisuzaki, J. Woollen, S.-K. Yang, J. J. Hnilo, M. Fiorino, and G. L. Potter (2002), NCEP-DOE AMIP-II Reanalysis (R-2), *Bull. Am. Meteorol. Soc.*, *83*, 1631–1643.

Kiehl, J. T. (1994), On the observed near cancellation between longwave and shortwave cloud forcing in tropical regions, *J. Clim.*, *7*, 559–565.

Lau, K.-M., C.-H. Sui, and W.-K. Tao (1993), A preliminary study of the tropical water cycle using the Goddard cumulus ensemble model, *Bull. Am. Meteorol. Soc.*, *74*, 1313–1321.

Lau, K.-M., C.-H. Sui, M.-D. Chou, and W.-K. Tao (1994), Cirrus cloud thermostat effect for tropical sea surface temperature-fact or fiction, *Geophys. Res. Lett.*, *21*, 1157–1160.

Li, X., C.-H. Sui, K.-M. Lau, and M.-D. Chou (1999), Large-scale forcing and cloud-radiation interaction in the tropical deep convective regime, *J. Atmos. Sci.*, *56*, 3028–3042.

Li, X., C.-H. Sui, and K.-M. Lau (2002), Dominant cloud microphysical processes in a tropical oceanic convective system: A 2-D cloud resolving modeling study, *Mon. Weather Rev.*, *130*, 2481–2491.

Lindzen, R. S. (1990), Some coolness concerning global warming, *Bull. Am. Meteorol. Soc.*, *71*, 288–299.

Lindzen, R. S., M.-D. Chou, and A. Hou (2000), Does the earth have an adaptive infrared iris?, *Bull. Am. Meteorol. Soc.*, *82*, 417–432.

Pierrehumbert, R. T. (1995), Thermostats, radiator fins, and the local runaway greenhouse, *J. Atmos. Sci.*, *52*, 1784–1806.

Prabhakara, C., D. P. Kratz, J.-M. Yoo, G. Dalu, and A. Vernekar (1993), Optically thin cirrus clouds: Radiative impact on the warm pool, *J. Quant. Spectrosc. Radiat. Transfer*, *49*, 467–483.

Ramanathan, V., and W. Collins (1991), Thermodynamic regulation of ocean warming by cirrus clouds deduced from observations of the 1987 El Nino, *Nature*, *351*, 27–32.

Reynolds, R. W., and T. S. Smith (1994), Improved global sea surface temperature analysis using optimum interpolation, *J. Clim.*, *7*, 929–948.

Soden, B. J. (1997), Variations in the tropical greenhouse effect during El Nino, *J. Clim.*, *10*, 1050–1055.

Soong, S.-T., and Y. Ogura (1980), Response of tradewind cumuli to large-scale processes, *J. Atmos. Sci.*, *37*, 2035–2050.

Soong, S. T., and W. K. Tao (1980), Response of deep tropical cumulus clouds to mesoscale processes, *J. Atmos. Sci.*, *37*, 2016–2034.

Sui, C.-H., K.-M. Lau, W.-K. Tao, M. D. Chou, and J. Simpson (1993), Simulated water and radiation budgets in the tropics, *Proc. 20th Conf. on Hurricanes and Tropical Meteorol.*, 291–294.

Sui, C.-H., K.-M. Lau, W.-K. Tao, and J. Simpson (1994), The tropical water and energy cycles in a cumulus ensemble model. Part I: Equilibrium climate, *J. Atmos. Sci.*, *51*, 711–728.

Sui, C.-H., X. Li, and K.-M. Lau (1998), Radiative-convective processes in simulated diurnal variations of tropical oceanic convection, *J. Atmos. Sci.*, *55*, 2345–2357.

Tao, W.-K., and J. Simpson (1993), The Goddard Cumulus Ensemble model. Part 1: Model description, *Terr. Atmos. Oceanic Sci.*, *4*, 35–72.

Tao, W.-K., and S.-T. Soong (1986), A study of the response of deep tropical clouds to mesoscale processes: Three-dimensional numerical experiments, *J. Atmos. Sci.*, *43*, 2653–2676.

Tao, W.-K., J. Simpson, and M. McCumber (1989), An ice-water saturation adjustment, *Mon. Weather Rev.*, *117*, 231–235.

Tao, W.-K., J. Simpson, C.-H. Sui, C.-L. Shie, B. Zhou, K.-M. Lau, and M. Moncrieff (1999), On equilibrium states simulated by cloud-resolving models, *J. Atmos. Sci.*, *56*, 3128–3139.

Tao, W.-K., et al. (2003), Microphysics, radiation and surface processes in the Goddard Cumulus Ensemble model, *Meteorol. Atmos. Physics*, *82*, 97–137.

Tompkins, A. M., and G. C. Craig (1998), Radiative-convective equilibrium in a three-dimensional cloud ensemble model, *Q. J. R. Meteorol. Soc.*, *124*, 2073–2098.

Xu, K.-M., and D. A. Randall (1999), A sensitivity study of radiative-convective equilibrium in the tropics with a convection-resolving model, *J. Atmos. Sci.*, *56*, 3385–3400.

Zhang, M. H., R. D. Cess, and S. C. Xie (1996), Relationship between cloud radiative forcing and sea surface temperatures over the entire tropical oceans, *J. Clim.*, *9*, 1374–1384.

C.-H. Ho, School of Earth and Environmental Sciences, Seoul National University, Seoul, Korea.

K.-M. Lau, NASA/GSFC/Laboratory for Atmospheres, Greenbelt, MD, USA.

X. Li, NOAA/NESDIS/Center for Satellite Applications and Research, Camps Springs, MD, USA.

C.-H. Sui, Institute of Hydrological and Oceanic Sciences and Department of Atmospheric Sciences, National Central University, No. 300, Wu-Chuan Li, Jhongli City, Taoyuan county 32001, Taiwan. (sui@ncu.edu.tw)